A new approach to structural integrity assessment based on axial and radial diffusivities

Claudia A.M. Wheeler-Kingshott, PhD [a]
Olga Ciccarelli, MD, PhD [b]
Torben Schneider [a]
Daniel C. Alexander, PhD [c]
Mara Cercignani, PhD [d]

[a]NMR Research Unit, Queen Square MS Centre, Department of Neuroinflammation, UCL Institute of Neurology, London, UK
[b]NMR Research Unit, Queen Square MS Centre, Department of Brain Repair and Rehabilitation, UCL Institute of Neurology, London, UK
[c]UCL Centre for Medical Image Computing, Department of Computer Science, University College London, London, UK
[d]Clinical Imaging Sciences Centre, Brighton & Sussex Medical School, Brighton, East Sussex, UK

Correspondence to: Claudia Wheeler-Kingshott
UCL Institute of Neurology
Queen Square, London, WC1N 3BG, UK
E-mail: c.wheeler-kingshott@ion.ucl.ac.uk

Summary
This study describes a method for performing diffusivity measures along and across a specific direction, derived from white matter in healthy controls. The diffusion tensor (DT) assigns a principal eigenvector (v_1) and eigenvalue (axial diffusivity, d_{ax}) to each voxel. The average of the second and third eigenvalues is the radial diffusivity, d_{rad}. v_1 may be affected by pathology, therefore when comparing d_{ax} and d_{rad} in patients one has to consider the direction of the measurement and underlying anatomy. Here we created a representative super-DT dataset, DT_{ref}, whose eigenvector, $v_{1,ref}$, was considered the most likely direction of diffusivity per voxel. We defined the projected axial diffusivity, $d_{p\text{-}ax}$, as the projection of individual DTs along $v_{1,ref}$ and the projected radial diffusivity, $d_{p\text{-}rad}$, as the average of the projections along the second and third eigenvectors of DT_{ref}. The projected diffusivities are promising new parameters for studying white matter pathology.

KEY WORDS: axial diffusivity, diffusion tensor, DTI, eigenvalues, radial diffusivity, template

Introduction

Magnetic resonance imaging (MRI) can be made sensitive to the displacement of water molecules in tissue *in vivo* and, under appropriate conditions, this displacement can be approximated with a Gaussian model, representing the overall effect as a diffusion tensor (DT). This allows the definition of three unique vectors, the *eigenvectors* of the DT, $\mathbf{v}_1$, $\mathbf{v}_2$ and $\mathbf{v}_3$, which represent the diffusivity along the principal direction and two orthogonal ones per each image voxel. Associated with these eigenvectors there are values corresponding to the apparent diffusion coefficient of the water molecules in each voxel along the direction of the eigenvectors. These diffusivities are known as the *eigenvalues* of the DT, λ_1, λ_2 and λ_3(1).

Axial and radial diffusivities, i.e. the water diffusion coefficient measured along and across axons, have been associated with the principal eigenvalue of the DT, λ_1, and the average of its orthogonal components, λ_2 and λ_3 (2). This is an acceptable approximation if the voxel contains a healthy fibre bundle that determines the diffusion properties of the voxel, but can lead to misinterpretation of the results if the signal-to-noise ratio (SNR) is low, or if crossing fibres are present, or if pathology causes a decrease in anisotropy. The latter situation occurs within brain lesions, such as those affecting the brain of patients with multiple sclerosis (MS) (3). Thus, in all these conditions the uncertainty associated with the definition of the principal direction of diffusion increases, i.e., $\mathbf{v}_1$ may be aligned with a direction other than that of the underlying "healthy" structure, as discussed in (4). In such voxels, comparing the eigenvalues of the DT between healthy controls and patients with lesions, such as those seen in MS, can be misleading because it corresponds effectively to comparing the diffusion coefficient along two different directions, hence representing different biological substrates.

This work proposes a new definition of the axial and radial diffusivities, which is consistent between subjects and independent of white matter focal pathology. This is achieved by calculating the diffusivity along directions that are defined in Montreal Neurological Institute (MNI) standard space, using a DT template generated from a control population.

Materials and methods

Subjects

Fifteen healthy controls (mean age 40±14 years, 6 females and 9 males) were scanned as the reference group (hcs). One additional healthy control (hc) (female, age 37 years) was included to be compared with the reference group, and two patients with a diagnosis of relapsing-remitting MS (5), p_1 (female, age 34 years, EDSS score = 2.5, disease duration = 1.5 years, total lesion load = 1,480.55 mm^3) and p_2 (male, age 55 years, EDSS score = 5.5, disease duration = 7 years, total lesion load = 21,142.50 mm^3), were also scanned with the same protocol. All the subjects gave their informed, writ-

ten consent before the study, which was approved by the Joint Ethics Committee of the Institute of Neurology and the National Hospital for Neurology and Neurosurgery (London, UK).

MRI protocol

Dual-Echo Fast Spin-Echo (DE-FSE)

Axial images, aligned to run parallel to a line that joins the most inferoanterior and inferoposterior parts of the corpus callosum (anterior commissure – posterior commissure: AC-PC line) were acquired with standard parameters (TE = 30/105 ms; TR = 2500 ms; number of slices = 28 contiguous; voxel size = 0.94 x 0.7 x 5 mm^3).

Diffusion Tensor Imaging (DTI)

A single-shot cardiac-gated diffusion-weighted spin-echo echo-planar imaging (DW-SE-EPI) sequence was run with the following parameters: TE = 0.096 s, TR = 20RR (≈20 s), 2.3x2.3x2.3 10^{-9} m^3 voxel size, 60 contiguous slices, aligned with the AC-PC line, 68 volumes of which 61 acquired with equally distributed (6) diffusion-weighted directions and b = 1200 10^6 s m^{-2} plus 7 volumes acquired with b = 0.

Processing pipeline

This section describes the steps taken to obtain a "super-DTI" control dataset in MNI space, which was used as a representative template for determining the main direction of diffusivity in each voxel for the healthy population. This super-DTI control dataset was used as the reference to define two new parameters, called "projected axial diffusivity", $d_{p\text{-}ax}$, and "projected radial diffusivity", $d_{p\text{-}rad}$. These new parameters were then compared on a voxel-by-voxel basis between i) the 15 hcs and the extra hc (whose scans were not used for the super-DTI dataset), and ii) the 15 hcs and the two MS patients, p_1 and p_2. The processing pipeline is also schematically represented in figure 1.

Definition of the reference axial and radial diffusivities

• DTI data from 15 healthy subjects were used to create a super-DTI dataset (7). For each subject, j, the DT was reconstructed voxelwise in native space using the Camino toolkit [http://www.camino.org.uk (8)] and diagonalised to produce traditional DTI metrics, including fractional anisotropy (FA_j), axial ($d_{ax,j}$) and radial ($d_{rad,j}$) diffusivities, where the axial diffusivity is assumed to coin-

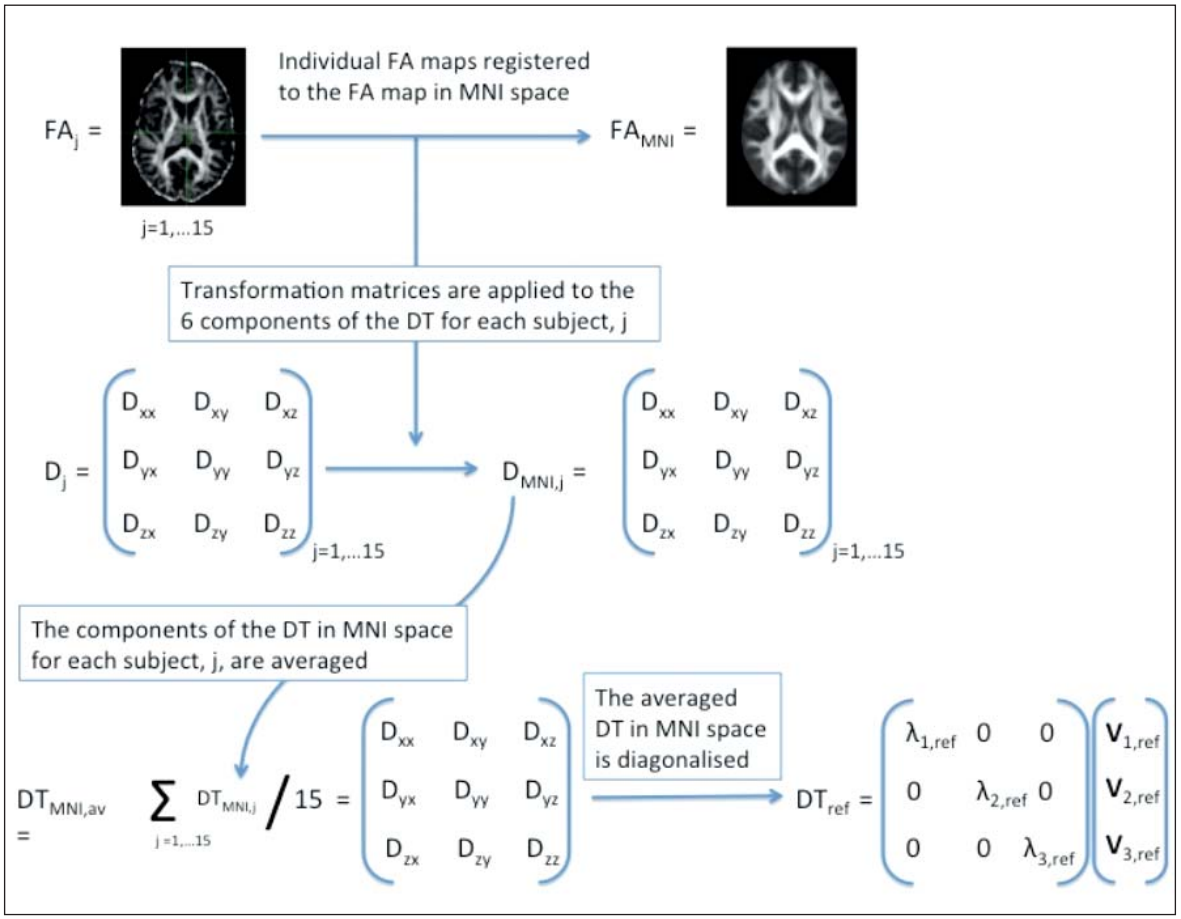

Figure 1 - Diagram of the pipeline used to obtain the super-DTI dataset and to calculate the projected axial and radial diffusivities, $d_{p\text{-}ax}$ and $d_{p\text{-}rad}$, for an individual subject.

cide with the principal eigenvalue of the DT_j of subject j, $\lambda_{1,j}$, while the radial diffusivity is associated with the average of the second and third eigenvalues, $\lambda_{2,j}$ and $\lambda_{3,j}$.

• For each subject j the FA_j map in native space was registered to the FA template from the Oxford Centre for Functional MRI of the Brain (FMRIB) library, FA_{MNI}, using first FLIRT, an affine registration step, followed by FNIRT, a non-linear registration algorithm, from the FSL toolkit (see FLIRT and FNIRT, http://www.fmrib.ox.ac.uk/fsl/fsl/list.html). The voxel resolution of the registered FA map matched the resolution of FA_{MNI}, i.e. 1x1x1 mm^3. The transformation matrix was then applied to the non-diagonalised diffusion tensor components, DT_j, using the preservation of principal direction (PPD) algorithm to reorient the DTs (9), providing a DT in MNI space, $DT_{MNI,j}$, for each subject j.

• Before diagonalisation, the $DT_{MNI,j}$ were averaged to produce a non-diagonalised super-DTI dataset, $DT_{MNI,av}$.

• $DT_{MNI,av}$ was subsequently diagonalised to obtain the diagonalised reference dataset, DT_{ref}, which gave us the three reference *eigenvectors*, $\mathbf{v}_{1,ref}$, $\mathbf{v}_{2,ref}$, $\mathbf{v}_{3,ref}$, and their corresponding *eigenvalues*, $\lambda_{1,ref}$, $\lambda_{2,ref}$, $\lambda_{3,ref}$ for each 1x1x1 mm^3 voxel.

• From the eigenvalues of DT_{ref} the FA map was calculated and used as the reference, FA_{ref}, for thresholding, assuming that voxels characterised by $FA_{ref}>0.3$ are most likely to be representative of white matter.

Definition of the projected axial and radial diffusivities

• For each subject we determined the component of the DT along each of the three eigenvectors of DT_{ref}, $\mathbf{v}_{1,ref}$, $\mathbf{v}_{2,ref}$, $\mathbf{v}_{3,ref}$, and we called these values the "projected" diffusivities: $d_{p1,j}$, $d_{p2,j}$, $d_{p3,j}$ where 1,2,3 indicates the projection along the first, second or third eigenvector of DT_{ref}, while j = 1…n indicates the subject investigated.
The projection of the DT of each subject j along $\mathbf{v}_{1,ref}$ is defined as the projected axial diffusivity for that subject, $d_{p\text{-}ax,j}$:

$$d_{p\text{-}ax,j} = (\mathbf{v}_{1,ref})^T \cdot DT_{MNI,j} \cdot (\mathbf{v}_{1,ref}) \quad \text{[eq 1]}$$

The average of the projections of the DT of each subject j along $\mathbf{v}_{2,ref}$ and $\mathbf{v}_{3,ref}$ was also calculated and defined as the projected radial diffusivity for subject j, $d_{p\text{-}rad,j}$:

$$d_{p\text{-}radj} = ((\mathbf{v}_{2,ref})^T \cdot DT_{MNI,j} \cdot (\mathbf{v}_{2,ref}) + (\mathbf{v}_{3,ref})^T \cdot DT_{MNI,j} \cdot (\mathbf{v}_{3,ref}))/2 \quad \text{[eq 2]}$$

Voxel-based morphometry (VBM) analysis of $\mathbf{d_{p\text{-}ax}}$ *and* $\mathbf{d_{p\text{-}rad}}$

• First, in the group of 15 hcs used for the super-DTI dataset we compared the axial diffusivity (d_{ax}) with the projected axial diffusivity ($d_{p\text{-}ax}$), and the radial diffusivity (d_{rad}) with the projected radial diffusivity ($d_{p\text{-}rad}$) using a paired-sample t-test in SPM5 (http://www.fil.ion.ucl.ac.uk/spm/software/spm5/).
• Second, we investigated differences in $d_{p\text{-}ax}$ and $d_{p\text{-}rad}$ between the 15 hcs and both i) the single healthy control (hc), and ii) the two patients with MS, p_1 and p_2, using a two sample t-test in SPM5. In particular, one group was set to be either hc, p_1 or p_2, while the other was set to be the hcs (i.e. the 15 healthy subjects used for the super-DTI dataset). Equality of variance for the two groups was assumed. We tested whether $d_{p\text{-}ax}$ and $d_{p\text{-}rad}$ of hc, p_1 and p_2 differed from the healthy population, and whether these differences overlapped with those obtained by comparing d_{ax} and d_{rad}, calculated from the DT, between subject groups.

MS lesions and axial and radial diffusivities

• Masks of the T_2-hyperintense MS lesions were drawn by an experienced neurologist (OC) on the proton-density-weighted scans of the DE-FSE dataset for both patients, p_1 and p_2;
• The T_2-weighted scans were then linearly registered to the b_0 scan of the super-DTI dataset via an affine transformation using FLIRT from the FSL library;
• The transformation coefficients from T_2 to b_0 space were subsequently combined with the non-linear transformation coefficients obtained from the non-linear registration of the individual FA maps to FA_{MNI};
• The combined transformation was applied to the original lesion mask file in order to have the lesion masks co-registered with the DTI matrices in MNI space.

Results

By definition, $d_{p\text{-}ax}$ is never greater than d_{ax} and $d_{p\text{-}rad}$ is never smaller than d_{rad}. With this in mind, these are the main findings of our study:

Voxel-based analysis of $\mathbf{d_{p\text{-}ax}}$ *and* $\mathbf{d_{p\text{-}rad}}$

HEALTHY CONTROLS

VBM comparisons of $d_{p\text{-}ax}$ with d_{ax} and $d_{p\text{-}rad}$ with d_{rad} of the 15 healthy volunteers, used for creating the super-DTI dataset, show areas of decreased $d_{p\text{-}ax}$ compared with d_{ax}; these areas overlap with regions showing an increased $d_{p\text{-}rad}$ compared with the corresponding values of d_{ax}, (see Fig. 2a, over).

AXIAL DIFFUSIVITY IN HC, P_1 AND P_2

The most remarkable result of the analysis is that p_2 (the patient with the highest clinical disability and highest total lesion load) shows areas of *decreased* projected axial diffusivity, $d_{p\text{-}ax}$, compared with the hcs. These areas are not always highlighted when looking at the differences in d_{ax} between this patient and the hcs, and often appear to extend beyond these regions (Fig. 2b, over), indicating that projected axial diffusivity may be sensitive to pathology in a different way from the axial diffusivity parameter. On the other hand, p_1 shows only a few voxels characterised by a reduced $d_{p\text{-}ax}$, which mostly coincide with voxels of reduced d_{ax} and are typically of limited spatial extent (Fig. 2c, over). No voxels of decreased $d_{p\text{-}ax}$ and d_{ax} are found in the hc when compared with the healthy population.
Areas of *increased* $d_{p\text{-}ax}$ compared with the hcs are also found in both patients; these regions do not always overlap with regions of increased d_{ax} and, in some locations, extend beyond them, especially in p_2 (Fig. 2d, over).

RADIAL DIFFUSIVITY IN HC, P_1 AND P_2

In contrast with the axial diffusivity results, the observed regions of *increased* $d_{p\text{-}rad}$ mostly coincide with regions of *increased* d_{rad}. In particular, the areas of difference in $d_{p\text{-}rad}$ between hc and p_1 and the healthy population (hcs) are almost identical to the regions obtained when comparing d_{rad} between these groups. Instead, p_2 shows regions of *increased* $d_{p\text{-}rad}$ when compared with hcs that coincide with areas of *increased* d_{rad}, but are spatially more localised (Fig. 2e). No areas of significant *decreased* radial diffusivities, $d_{p\text{-}rad}$ or d_{rad}, are found in any of the subjects, hc, p_1 and p_2, and hcs.

MS lesions and axial and radial diffusivities

The location of the white matter lesions of p_1 and p_2 was compared with the areas of *increased* radial diffusivity, *increased* axial diffusivity and *decreased* axial diffusivity, for both the traditionally defined parameters, d_{ax} and d_{rad}, and the projected parameters, $d_{p\text{-}ax}$ and $d_{p\text{-}rad}$. Figure 2f shows the relative position of lesions and areas of changes for p_2.

Areas of *increased* $d_{p\text{-}rad}$ and d_{rad}, observed in p_2 when compared with hcs, overlap with lesions identified on T_2-weighted scans and also extend beyond their boundaries (Fig. 2f-1). Areas of *increased* $d_{p\text{-}ax}$ and d_{ax} observed in p_2 are localised within the lesion mask (Fig. 2f-2), while areas of *decreased* axial diffusivity in p_2 are not always related to the presence of focal lesions, but are also seen outside the focal lesions, in the normal-appearing white matter (Fig. 2f-3).

Discussion

We have defined two new parameters to be used for evaluating the diffusion coefficient of water molecule displacement along and across axons. We have called these parameters "projected axial" diffusivity, $d_{p\text{-}ax}$, and "projected radial" diffusivity, $d_{p\text{-}rad}$. They are obtained by calculating the component of the DT along a specific direction, defined as the direction of the principal eigenvector of a "super-DT" dataset, built from 15 hcs. In fact, it is well known that pathology can change the alignment of the eigenvectors of the DT with respect to the underlying tissue structure, and can also reflect actual changes in the tissue structures if invasive pathology is present, as in the case of tumours (10). If the first case, such as in MS in which white matter is affected by non-ex-

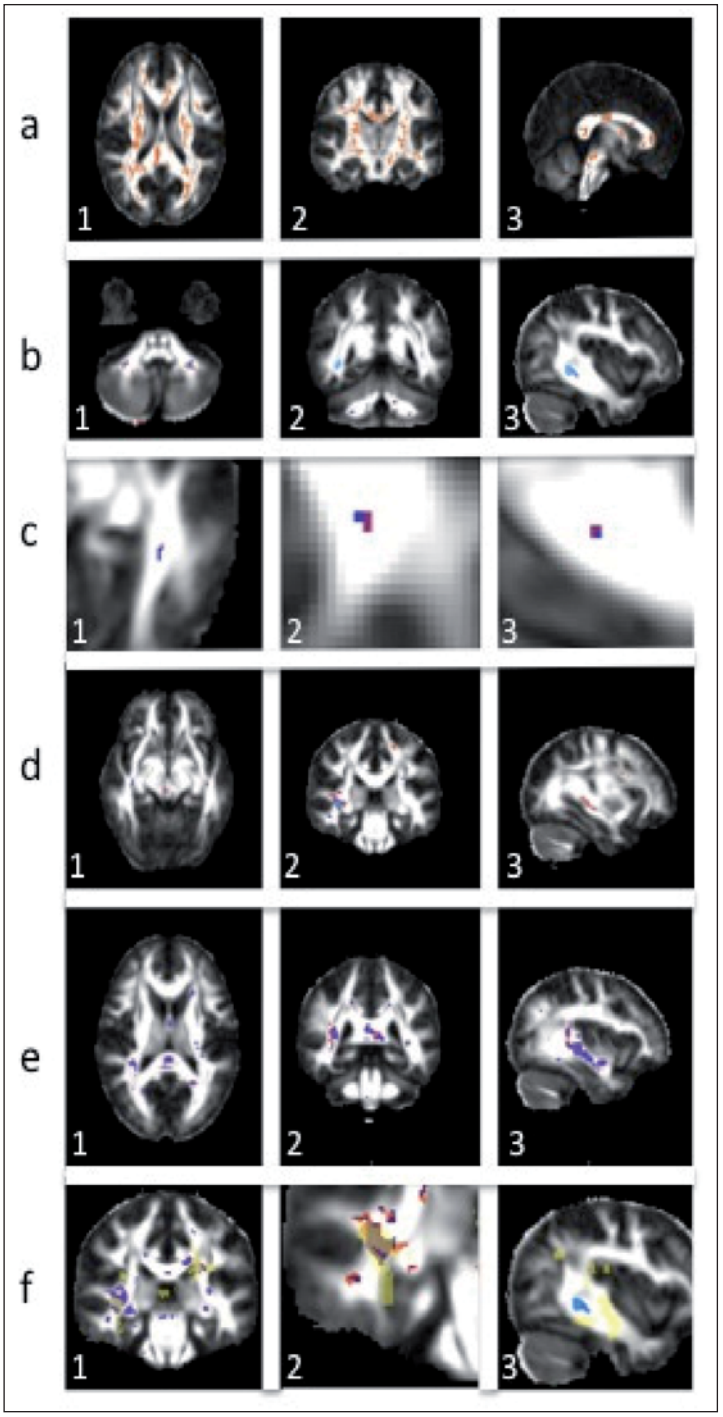

Figure 2 - a) Axial, coronal and sagittal views of fractional anisotropy with areas of increased projected radial, $d_{p\text{-}rad}$, compared with radial, d_{rad}, diffusivity and decreased projected axial, $d_{p\text{-}ax}$, compared with axial, d_{ax}, diffusivity in a population of 15 healthy controls; b) Areas of decreased projected axial diffusivity in p_2, $d_{p\text{-}ax,p2}$, shown in blue, overlaid on areas of decreased axial diffusivity, $d_{ax,p2}$, shown in red. c) The same as b) but for p_1; d) Areas of increased projected axial, $d_{p\text{-}ax,p2}$, (blue) and axial, $d_{ax,p2}$, (red) diffusivity in p_2; e) Areas of increased projected radial, $d_{p\text{-}rad,p2}$, (blue) and axial, $d_{rad,p2}$, (red) diffusivity in p_2; f) Overlay of areas of axial and radial diffusivity changes and lesion localisation (yellow) in p_2. 1 – areas of increased $d_{p\text{-}rad,p2}$ (blue) and $d_{rad\text{-}p2}$ (red); 2 – areas of increased $d_{p\text{-}ax,p2}$ (blue) and $_{dax\text{-}p2}$ (red); 3 – areas of decreased $d_{p\text{-}ax,p2}$ (blue) and $d_{ax\text{-}p2}$ (red). In all images, purple voxels are common voxels of changes in the projected and standard diffusivities.

pansive lesions of a degenerative nature (11), the principal eigenvalue of the diseased brain may not reflect the same biophysical substrate as the principal eigenvalue of a healthy brain, as shown by Wheeler-Kingshott and Cercignani (4). The new parameters, $d_{p\text{-}ax}$ and $d_{p\text{-}rad}$, therefore, aim to provide a means of evaluating possible changes along and across the most probable direction of healthy white matter fibres.

A reference DT dataset was built using data from 15 hcs and a non-linear registration algorithm to transform individual FA maps into MNI space. The registration of white matter structures was visually checked using reference landmarks. We applied the transformations to the individual components of each subject's DT, applying the PPD algorithm to reorient the DTs. Peng et al. (12) adopted a similar approach: these authors used a large population of healthy subjects to create a high-resolution high-SNR DT dataset, using data acquired with Turboprop-DTI instead of the more commonly available and used DW-SE-EPI. The dependence of the resulting DT dataset on the population used for the averaged template remains to be tested. Also, it is known that there is an effect of age on the DT properties; for this reason, we, too, believe that building a specific template for each study will allow the use of an age- and gender-matched population for the super-DT control dataset.

Due to the low FA of grey matter structures and therefore the potential errors in inter-subject non-linear registration of grey matter voxels based on their FA maps, we decided to select only voxels characterised by FA greater than 0.3, on the assumption that they correspond mainly to white matter areas.

This paper presents a new method for analysing axial and radial diffusivities and also provides an example of its application to patients with MS, which causes the development of focal brain lesions, as well as widespread white matter damage. Voxel-based group mapping is typically used to compare two populations of subjects of similar size, with smoothing of the data ensuring that the model's error terms are normally distributed. This assumption is violated when voxel-based analysis is used to investigate differences between a single subject and a control group, therefore results of this analysis need to be carefully interpreted as false positives may occur (13). A similar approach has been previously utilized elsewhere (14). With this consideration in mind this method can be used in future to assess, *in vivo*, the microstructural damage occurring in other neurological diseases that lead to neurodegeneration, such as amyotrophic lateral sclerosis, which is now regarded as a multisystem disorder in which the motor neurons are affected earliest and most severely (15). Other neurodegenerative diseases that would benefit from the application of this method are those that fall into the category of the tauopathies, such as corticobasal degeneration and progressive supranuclear palsy; it would be interesting to test whether this method can help in the differential diagnosis between these diseases and Parkinson's disease (16), on the basis of the differences in microstructural correlates detected with axial and radial diffusivity analysis.

In this study we first compared the projected diffusivities, $d_{p\text{-}ax}$ and $d_{p\text{-}rad}$, with d_{ax} and d_{rad}, i.e. the axial and radial diffusivities defined from the eigenvalues of the DT, in the healthy population used for the super-DTI dataset. Because of individual normal variability even in core areas of white matter tracts, we found, not surprisingly, that several areas showed $d_{p\text{-}ax}$ lower than d_{ax} and $d_{p\text{-}rad}$ higher than d_{rad} (Fig. 2a). We then investigated changes in the new projected parameters between three further individual examples, i.e. hc, p_1 and p_2, and the 15 hcs, thus showing the potential clinical applications of $d_{p\text{-}ax}$ and $d_{p\text{-}rad}$. These are the same subjects used in a previous publication (4), which demonstrated the weakness of the axial and radial diffusivities defined from the eigenvalues of the DT. By definition, $d_{p\text{-}ax}$ is never higher than the corresponding d_{ax} measured in the same subject. When we report areas of increased $d_{p\text{-}ax}$ these refer to individual subjects compared to the reference super-DT dataset. Equally, by definition $d_{p\text{-}rad}$ is never smaller than the corresponding d_{rad}, measured in the individual subject.

When comparing $d_{p\text{-}ax}$ and $d_{p\text{-}rad}$ of the single hc, not included in the super-DT dataset, with the population of hcs, we did not find any area showing statistically significant differences, which indicates that the subject's eigenvectors are aligned with the super-DTI template. When comparing the patient with the lowest disability and lowest lesion load (p_1) with the hcs, we observed only sparse and small areas showing differences in the new proposed parameters (Fig. 2c). Also, these areas were very similar to, and mostly coincided with, the regions obtained by the same analysis using the standard parameters, d_{ax} and d_{rad}, confirming that in healthy brain tissue and in the presence of *mild* tissue disruption the eigenvalues of the DT are suitable indicators of disease progression. This also means that in this case the eigenvectors of the DT are within the dispersion of the directions of the eigenvectors in the hcs used for the super-DTI template. The new parameters, though, give extra information when the pathology is more advanced, as in p_2, showing for example areas of normal-appearing white matter characterised by a reduced $d_{p\text{-}ax}$ not shown by d_{ax}. This reduced projected axial diffusivity is likely to derive from a reduced precision of the principal direction in the affected areas, which causes a misalignment with the reference principal diffusivity and therefore a lower $d_{p\text{-}ax}$.

The sensitivity of $d_{p\text{-}ax}$ and $d_{p\text{-}rad}$ to pathology needs to be confirmed, but our preliminary findings suggest that in the presence of a more severe pathology the comparisons show a more complex picture. In fact, we found in p_2 i) regions where a lesion overlapped almost perfectly with areas of both $d_{p\text{-}ax}$ and $d_{p\text{-}rad}$ changes; ii) areas where a lesion covered a subregion of $d_{p\text{-}ax}$ and $d_{p\text{-}rad}$ changes; iii) areas where there was a change of either $d_{p\text{-}ax}$ or $d_{p\text{-}rad}$ outside the lesion; iv) regions where lesions were not accompanied by changes in the diffusivities.

The comparisons between the standard and newly proposed parameters showed that:

Radial diffusivity: i) areas of *increased* radial diffusivity overlap a portion of the lesions and extend beyond the lesions to normal-appearing white matter tissue (Fig. 2f-1); looking at the distribution of the affected voxels, it is apparent that in general $d_{p\text{-}rad}$ is more spatially localised than d_{rad} in p_2, while in p_1 the two quantities extend over very similar voxels; ii) there are no areas of *decreased* radial diffusivities compared with hcs.

Axial diffusivity: i) the core of some lesions is accompanied by an *increase* of both d_{ax} and $d_{p\text{-}ax}$ with only a slight difference in the extent of coverage of the area highlight-

ed by the two diffusivity parameters (Fig. 2f-2); ii) most strikingly, $d_{p\text{-}ax}$ shows areas of *decreased* diffusivity (Fig. 2f-3) highlighting areas of degeneration not shown by d_{ax}. This is particularly evident in p_2, but small areas of *decreased* $d_{p\text{-}ax}$ are also present in p_1, while there are none in hc.

The pathological substrate of the projected axial and radial diffusivities needs to be confirmed with an appropriate post-mortem study. The design of such a study is not straightforward given the need to have a reference healthy template for the brain used for the registration, therefore whole-brain high-resolution acquisitions are recommended. Previous work on axial and radial diffusivities has used animal models to test the hypothesis that d_{ax} changes reflect axonal damage while d_{rad} changes are related to myelin breakdown and remyelination. In fact, Song et al., in an animal model of optic nerve retinal ischaemia (17), found that axial diffusivity, d_{ax}, was decreased and correlated with axonal degeneration in the absence of myelin breakdown. An increase in radial diffusivity, d_{rad}, was instead observed with the occurrence of myelin breakdown. A subsequent study of d_{ax} and d_{rad} in the corpus callosum of a mouse brain after cuprizone treatment (18) confirmed that d_{rad} is a marker of demyelination (increase) and subsequent remyelination (decrease). In this model Song et al. also observed a decrease in d_{ax} in conjunction with axonal damage, but the change did not reach statistical significance. In order to validate the biological substrate of $d_{p\text{-}ax}$ and $d_{p\text{-}rad}$, in animal models, similarly to what has been done for d_{ax} and d_{rad}, one would need to acquire data on healthy animals first in order to be able to define a standard template to use as a healthy reference dataset. At present, on the basis of our current analysis of *in vivo* human data, we propose that the projected axial diffusivity, $d_{p\text{-}ax}$, may be more sensitive to axonal damage than d_{ax} because of the observation that there are areas of decreased $d_{p\text{-}ax}$ where no d_{ax} changes occurred.

To assess their sensitivity to pathology, the new parameters can be studied in any patient population that is affected by white matter focal lesions. The projected axial and radial diffusivities cannot be used in cases where the pathology involves expansive lesions and disrupts white matter structures to the degree that registration to a template is not possible, as in the case of large and/or particularly invasive tumours, but in such cases it is strongly advisable not to analyse the eigenvalues of the DT either, because the direction of the eigenvectors becomes difficult to compare between time-points and between subjects, in relation to the underlying structures that they represent.

In conclusion, the projected axial and radial diffusivities not only have a more consistent interpretation than the axial and radial diffusivities calculated from the DT eigenvalues of the individual subject, but they also offer a new means of studying the evolution of degenerative pathologies such as MS.

Acknowledgements

The authors acknowledge the Multiple Sclerosis Society of Great Britain and Northern Ireland for supporting the NMR Unit with a generous programme grant, the UCLH/UCL Biomedical Research Centre, the EPSRC for supporting Prof. D. Alexander, and the International Spinal Research Trust for supporting Mr T Schneider.

References

1. Basser PJ, Pierpaoli C. A simplified method to measure the diffusion tensor from seven MR images. Magn Reson Med 1998;39:928-934
2. Song SK, Sun SW, Ramsbottom MJ, Chang C, Russell J, Cross AH. Dysmyelination revealed through MRI as increased radial (but unchanged axial) diffusion of water. Neuroimage 2002;17:1429-1436
3. Rovaris M, Agosta F, Pagani E, Filippi M. Diffusion tensor MR imaging. Neuroimaging Clin N Am 2009;19:37-43
4. Wheeler-Kingshott CA, Cercignani M. About "axial" and "radial" diffusivities. Magn Reson Med 2009;61:1255-1260
5. McDonald WI, Compston A, Edan G et al. Recommended diagnostic criteria for multiple sclerosis: guidelines from the International Panel on the diagnosis of multiple sclerosis. Ann Neurol 2001;50:121-127
6. Cook PA, Symms M, Boulby PA, Alexander DC. Optimal acquisition orders of diffusion-weighted MRI measurements. J Magn Reson Imaging 2007;25:1051-1058
7. Tozer DJ, Chard DT, Bodini B et al. Linking white matter tracts to associated cortical grey matter: a tract extension methodology. Neuroimage 2012;59:3094-3102
8. Cook PA, Bai Y, Nedjati-Gilani K et al. Camino: Open-Source Diffusion-MRI Reconstruction and Processing. Proceedings of the International Society for Magnetic Resonance in Medicine 2006;14:2759
9. Alexander DC, Pierpaoli C, Basser PJ, Gee JC. Spatial transformations of diffusion tensor magnetic resonance images. IEEE Trans Med Imaging 2001;20:1131-1139
10. Field AS, Alexander AL, Wu YC, Hasan KM, Witwer B, Badie B. Diffusion tensor eigenvector directional color imaging patterns in the evaluation of cerebral white matter tracts altered by tumor. J Magn Reson Imaging 2004;2:555-562
11. Dutta R, Trapp BD. Mechanisms of neuronal dysfunction and degeneration in multiple sclerosis. Prog Neurobiol 2011;93:1-12
12. Peng H, Orlichenko A, Dawe RJ, Agam G, Zhang S, Arfanakis K. Development of a human brain diffusion tensor template. Neuroimage 2009;46:967-980
13. Salmond CH, Ashburner J, Vargha-Khadem F, Connelly A, Gadian DG, Friston KJ. Distributional assumptions in voxel-based morphometry. Neuroimage 2002;17:1027-1030
14. Bozzali M, Cercignani M, Baglio F et al. Voxel-wise analysis of diffusion tensor MRI improves the confidence of diagnosis of corticobasal degeneration non-invasively. Parkinsonism Relat Disord 2008;14:436-439
15. Ferraiuolo L, Kirby J, Grierson AJ, Sendtner M, Shaw PJ. Molecular pathways of motor neuron injury in amyotrophic lateral sclerosis. Nat Rev Neurol 2011 ;7:616-630
16. Rizzo G, Martinelli P, Manners D et al. Diffusion-weighted brain imaging study of patients with clinical diagnosis of corticobasal degeneration, progressive supranuclear palsy and Parkinson's disease. Brain 2008;131:2690-2700
17. Song SK, Sun SW, Ju WK, Lin SJ, Cross AH, Neufeld AH. Diffusion tensor imaging detects and differentiates axon and myelin degeneration in mouse optic nerve after retinal ischemia. Neuroimage 2003;20:1714-1722
18. Song SK, Yoshino J, Le TQ et al. Demyelination increases radial diffusivity in corpus callosum of mouse brain. Neuroimage 2005;26:132-140